Advances in Applied Mathematics and Mechanics
Adv. Appl. Math. Mech., Vol. **15**, No. 6, pp. 1456-1472

DOI: 10.4208/aamm.OA-2022-0195
December 2023

Construction of Non-Equilibrium Gas Distribution Functions through Expansions in Peculiar Velocity Space

Z. Y. Yuan[1], Z. Chen[2], C. Shu[3,*], Y. Y. Liu[3] and Z. L. Zhang[3]

[1] *School of Energy and Power Engineering, Nanjing University of Science and Technology, Nanjing, Jiangsu 210094, China*
[2] *School of Naval Architecture, Ocean and Civil Engineering, Shanghai Jiao Tong University, Shanghai 200240, China*
[3] *Department of Mechanical Engineering, National University of Singapore, 10 Kent Ridge Crescent, 119260, Singapore*

Received 17 July 2022; Accepted (in revised version) 24 October 2022

Abstract. Gas distribution function plays a crucial role in the description of gas flows at the mesoscopic scale. In the presence of non-equilibrium flow, the distribution function loses its rotational symmetricity, making the mathematical derivation difficult. From both the Chapman-Enskog expansion and the Hermite polynomial expansion (Grad's method), we observe that the non-equilibrium effect is closely related to the peculiar velocity space (C). Based on this recognition, we propose a new methodology to construct the non-equilibrium distribution function from the perspective of polynomial expansion in the peculiar velocity space of molecules. The coefficients involved in the non-equilibrium distribution function can be exactly determined by the compatibility conditions and the moment relationships. This new framework allows constructing non-equilibrium distribution functions at any order of truncation, and the ones at the third and the fourth order have been presented in this paper for illustration purposes. Numerical validations demonstrate that the new method is more accurate than the Grad's method at the same truncation error for describing non-equilibrium effects. Two-dimensional benchmark tests are performed to shed light on the applicability of the new method to practical engineering problems.

AMS subject classifications: 76P05
Key words: Non-equilibrium gas distribution function, peculiar velocity space, complete polynomial expansion.

1 Introduction

The gas distribution function is a probability function to describe the molecular behaviors in the phase velocity space. It plays essential roles in modeling gas flows from the

*Corresponding author.
Email: mpeshuc@nus.edu.sg (C. Shu)

mesoscopic perspective in a way that the moments of the gas distribution function recover macroscopic flow variables such as density, velocity and temperature. In equilibrium state, the gas distribution function can be exactly derived as the Maxwellian distribution [1]. This distribution function is unimodal with Gaussian-like forms and possesses rotational symmetricity in the phase velocity space [2]. However, in the presence of non-equilibrium flows (e.g., the shock wave structure [3–5], asymmetric features such as bimodal forms arise in the distribution function, which increment the difficulties in constructing mathematical models.

Existing methods to approximate the distribution function for non-equilibrium flows stem from two ideas: the Chapman-Enskog (CE) expansion [6] and the Hermite polynomial expansion [7]. Specifically, the CE expansion performs power series expansion on the equilibrium distribution function [8–10]. With more expansion terms, the constructed distribution function is expected to more precisely describe the deviation from equilibrium state. However, since it is expanded with respect to a term proportional to the Knudsen number [11], this approach naturally fails in recovering strong non-equilibrium behaviors. To alleviate these limitations, Grad [12] approximated the non-equilibrium distribution function in terms of Hermite polynomial expansion. Among various versions of Grad's models, the Grad's 13 distribution function [12] truncating at the third-order Hermite polynomial expansion is perhaps the most classical one, whose capability is mainly recognized in the slip regime and the transition regime at moderate Knudsen number [13]. Stronger non-equilibrium behaviors can be recovered by using the fourth-order Hermite polynomial expansion, which results in Grad's 26 distribution function [14]. However, the Grad's distribution function is derived from the orthogonal Hermite polynomial expansion. As a result, it merely considers the contracted coefficients and contracted polynomials, which strictly satisfy orthogonality. The non-orthogonal terms are never considered and will lose some physical information to some extent.

Hence, it is still desirable to propose an effective distribution function, which could be more capable for the prediction of its shape in the non-equilibrium flows than the one derived from the CE expansion or Hermite polynomial expansion. Existing works show that the non-equilibrium distribution functions derived from CE expansion and Hermite polynomial expansion can be both formulated as an equilibrium distribution function multiplying a revision term ϕ. For the CE expansion method, the term ϕ^{CE} is associated with the gradients of thermodynamic variables and the peculiar velocities [15]. In the meantime, for the Grad's distribution function, the revision term ϕ^{Grad} is mainly made of the high-order moments and the peculiar velocities. Both perspectives imply that the non-equilibrium effect could be closely associated with the peculiar velocities, which leads to a natural question of whether the direct expansion in the peculiar velocity space could construct more accurate non-equilibrium terms. The answer towards this question motivates the present paper.

In this paper, we propose a generalized methodology to construct non-equilibrium gas distribution functions based on the complete polynomial expansion in the peculiar

velocity space $C=[C_1,C_2,C_3]$. The coefficients involved in the expansion are determined by the compatibility conditions and the moment relationships. Mathematically, this expansion can be carried out to infinite orders of C. In the present work, the constructed gas distribution function is truncated at the third and the fourth orders to illustrate the expansion process. At the same time, the third-order and the fourth-order truncations provide intuitive comparisons with Grad's 13 distribution function and Grad's 26 distribution function, which are truncated at the third and the fourth orders of Hermite polynomial expansion, respectively. Validations show that the new construction strategy outperforms the Grad's method at the same order of truncation in terms of describing non-equilibrium behaviors. Furthermore, distribution functions truncated at even higher order can be routinely constructed using the new method as per needs in the future studies.

2 The existing Maxwellian, Navier-Stokes and Grad's distribution functions

For the equilibrium flow, the distribution function of gas molecules follows the Maxwellian distribution [16]. More specifically, for monatomic gas, the distribution function reads

$$g=\rho/(2\pi RT)^{3/2}\cdot e^{-C^2/2RT}, \tag{2.1}$$

here, ρ is the macroscopic density, T denotes the macroscopic temperature. R is the gas constant. $C=[C_1,C_2,C_3]$ is the peculiar velocity vector, in which C_1, C_2 and C_3 are the components in the x-, y- and z-directions. In quasi-equilibrium flow regime, the distribution function can be derived by the CE expansion method. The first-order CE expansion [15,17] leads to the following distribution function that recovers Navier-Stokes (NS) flows

$$f^{NS}=g\phi^{NS}=g\left[1+\frac{C_iC_j}{2pRT}\left(-2\mu\frac{\partial U_{<i}}{\partial x_{j>}}\right)+\frac{C_i}{pRT}\left(\frac{C^2}{5RT}-1\right)\cdot\left(-\lambda\frac{\partial T}{\partial x_i}\right)\right], \tag{2.2}$$

where p is the pressure; $-2\mu\cdot\partial U_{<i}/\partial x_{j>}$ and $-\lambda\cdot\partial T/\partial x_i$ are equivalent to the linearized stress tensor and heat flux, respectively. Different from the NS distribution function, the Grad's 13 distribution function is established from the third-order truncated Hermite polynomial expansion [12], which gives

$$f^{G13}=g\phi^{G13}=g\left[1+\frac{\sigma_{ij}}{2pRT}C_iC_j+\frac{q_iC_i}{pRT}\left(\frac{C^2}{5RT}-1\right)\right], \tag{2.3}$$

where σ_{ij} denotes the stress tensor and q_i means the heat flux. Comparing the above equation with the form of NS distribution function shown in Eq. (2.2), we can see that

the heat flux and stress tensor in the Grad's distribution function are not explicitly given. They are determined by the moments of distribution function [18–20] as follows

$$\sigma_{ij}=\left\langle\left(C_iC_j-\frac{1}{3}\delta_{ij}C_kC_k\right)f\right\rangle,\quad q_i=\left\langle\frac{1}{2}C_iC^2f\right\rangle, \tag{2.4}$$

where $\langle\cdots\rangle$ means the integration over the whole velocity space and is calculated by,

$$\langle\cdots\rangle=\int_{-\infty}^{+\infty}\int_{-\infty}^{+\infty}\int_{-\infty}^{+\infty}(\cdots)d\xi_1d\xi_2d\xi_3. \tag{2.5}$$

3 Non-equilibrium gas distribution function constructed by complete expansion in the peculiar velocity space

By comparing Eq. (2.2) and Eq. (2.3), we can see that the non-equilibrium distribution function can be expressed in a general format of an equilibrium distribution function multiplying a non-equilibrium term,

$$f=g\phi, \tag{3.1}$$

where ϕ represents the non-equilibrium effect. For the NS distribution function in Eq. (2.2), the ϕ^{NS} mainly consists of gradients of thermodynamic variables and the peculiar velocities. The ϕ^{G13} in the Grad's 13 distribution function shown in Eq. (2.3), mainly consists of the high-order moments and the peculiar velocities. Hence, the peculiar velocities are essential elements in the construction of non-equilibrium term from both CE expansion and the Hermite polynomial expansion perspectives. A direct way of mathematically interpreting this vision is to construct the non-equilibrium factor ϕ through a complete expansion in the peculiar velocity space, given as,

$$\phi=\sum a_{mnl}C_1^mC_2^nC_3^l, \tag{3.2}$$

where a_{mnl} is the coefficient for the corresponding term. m, n and l stand for the power of each peculiar velocity component. Then, the format of non-equilibrium distribution function shown in Eq. (3.1) can be reformulated as,

$$f=g\cdot\sum a_{mnl}C_1^mC_2^nC_3^l, \tag{3.3}$$

Eq. (3.3) represents a general expression of this new exploration, in which all coefficients a_{mnl} should be properly derived. Here, we employ the compatibility conditions and the moment relationships which have been proven to be robust for various kinds of flows, no matter whether the flow is in the equilibrium state or in the non-equilibrium state. The compatibility conditions yield

$$\langle f\rangle=\langle g\rangle=\rho,\quad\langle f\xi_i\rangle=\langle g\xi_i\rangle=\rho U_i,\quad\left\langle f\cdot\frac{1}{2}\xi_i^2\right\rangle=\left\langle g\cdot\frac{1}{2}\xi_i^2\right\rangle=\rho E, \tag{3.4}$$

where $E=1/2\cdot\rho U^2+3\rho RT/2$ is the energy. The moment relationships give

$$\left\langle C_1^m C_2^n C_3^l f\right\rangle=\left\langle g\cdot\sum a_{mnl}C_1^m C_2^n C_3^l\right\rangle. \tag{3.5}$$

It is noteworthy that the more expansions conducted, the more equations of the moment relationships can be obtained. Although the expansion in the peculiar velocity can be made to infinite orders, it is unreal to solve a system containing infinite equations. A practical method is to truncate the expansion terms at certain order. In this paper, the expansion in the peculiar velocity will be truncated at the third-order and the fourth-order for illustration.

4 Distribution function derived from the third-order truncation

The truncation of ϕ at the third-order means that $m+n+l\leq 3$ and $m,n,l\in N$. Taking the one-dimensional case as an example, the terms containing odd powers of C_2 or C_3 vanish, and thus the non-equilibrium term can be expanded as,

$$\phi^{3rd}=a_{000}+a_{100}C_1+a_{200}C_1^2+a_{020}C_2^2+a_{002}C_3^2+a_{300}C_1^3+a_{120}C_1C_2^2+a_{102}C_1C_3^2. \tag{4.1}$$

The above expression involves eight unknown coefficients. The compatibility conditions in Eq. (3.4) give the following relations for the 1-D case

$$\langle f\rangle=\langle g\rangle=\rho,\quad \langle f\xi_1\rangle=\langle g\xi_1\rangle=\rho U_1,\quad \left\langle f\cdot\frac{1}{2}\xi_i^2\right\rangle=\left\langle g\cdot\frac{1}{2}\xi_i^2\right\rangle=\rho E. \tag{4.2}$$

By substituting $\xi_i=U_i+C_i$ into Eq. (4.2), the compatibility conditions can be reformulated as

$$\langle f\rangle=\rho,\quad \langle fC_1\rangle=0,\quad \left\langle f\cdot C^2\right\rangle=3\rho RT. \tag{4.3}$$

Substituting $f=g\phi^{3rd}$ into Eq. (4.3) gives

$$a_{000}=1,\quad a_{200}+a_{020}+a_{002}=0,\quad a_{100}+(3a_{300}+a_{120}+a_{102})\cdot(RT)=0. \tag{4.4}$$

Then, considering the different orders in the moment relationships in Eq. (3.5), we can derive the following relations

$$\left\langle C_1^2 f\right\rangle=\rho RT\left(a_{000}+3RTa_{200}+RTa_{020}+RTa_{002}\right), \tag{4.5a}$$
$$\left\langle C_2^2 f\right\rangle=\rho RT\left(a_{000}+RTa_{200}+3RTa_{020}+RTa_{002}\right), \tag{4.5b}$$
$$\left\langle C_3^2 f\right\rangle=\rho RT\left(a_{000}+RTa_{200}+RTa_{020}+3RTa_{002}\right), \tag{4.5c}$$
$$\left\langle C_1^3 f\right\rangle=3\rho(RT)^2\left[a_{100}+RT(5a_{300}+a_{120}+a_{102})\right], \tag{4.5d}$$
$$\left\langle C_1C_2^2 f\right\rangle=\rho(RT)^2\left[a_{100}+RT(3a_{300}+3a_{120}+a_{102})\right], \tag{4.5e}$$
$$\left\langle C_1C_3^2 f\right\rangle=\rho(RT)^2\left[a_{100}+RT(3a_{300}+a_{120}+3a_{102})\right]. \tag{4.5f}$$

Finally, combining the compatibility conditions shown in Eq. (4.4) and the moment relationships in Eqs. (4.5a)-(4.5f), the coefficients in Eq. (4.1) can be determined as

$$a_{000}=1, \qquad a_{100}=-\frac{\langle C_1C^2f\rangle}{2\rho(RT)^2}, \tag{4.6a}$$

$$a_{200}=\frac{\langle C_1^2f\rangle}{2\rho(RT)^2}-\frac{1}{2RT}, \quad a_{020}=\frac{\langle C_2^2f\rangle}{2\rho(RT)^2}-\frac{1}{2RT}, \quad a_{002}=\frac{\langle C_3^2f\rangle}{2\rho(RT)^2}-\frac{1}{2RT}, \tag{4.6b}$$

$$a_{300}=\frac{\langle C_1^3f\rangle}{6\rho(RT)^3}, \quad a_{120}=\frac{\langle C_1C_2^2f\rangle}{2\rho(RT)^3}, \quad a_{102}=\frac{\langle C_1C_3^2f\rangle}{2\rho(RT)^3}. \tag{4.6c}$$

Now we validate the accuracy of the new distribution function by comparing it with the Grad's 13 distribution function. A benchmark non-equilibrium distribution function is produced by combining two equilibrium distribution function at different states, which gives

$$f^{neq}=\rho_1/(2\pi RT_1)^{3/2}\cdot e^{-C^2/2RT_1}+\rho_2/(2\pi RT_2)^{3/2}\cdot e^{-C^2/2RT_2}. \tag{4.7}$$

To generalize, the density, velocity and temperature involved in the Maxwellian distribution function are normalized as,

$$\hat{\rho}=\frac{\rho}{\rho_\infty}, \quad \hat{U}=\frac{U}{U_\infty}, \quad \hat{T}=\frac{T}{T_\infty}, \tag{4.8}$$

where ρ_∞=$1kg/m^3$ is the reference density, T_∞=$273K$ is the reference temperature, and U_∞=$\sqrt{2RT_\infty}$=$337m/s$ is the reference velocity. R is equal to $208J/kgK$ for argon gas. Since the Mach number is defined as $Ma=U/\sqrt{\gamma RT_\infty}$, the dimensionless velocity can be written as $\hat{U}$=$Ma\sqrt{\gamma/2}$, where the specific heat ratio γ is equal to $5/3$ for argon gas. Here we fix the parameters $\hat{\rho}_1=1$, $Ma_1=0$, $\hat{T}_1=1$ and consider three different cases: (a) $\hat{\rho}_2=2$, $Ma_2=1.5$, $\hat{T}_2=1$, (b) $\hat{\rho}_2=2$, $Ma_2=2$, $\hat{T}_2=1$, (c) $\hat{\rho}_2=2$, $Ma_2=2.5$, $\hat{T}_2=1$. For each case, the non-equilibrium distribution function can be calculated from Eq. (4.7) using specified macroscopic variables. The stress tensor and heat flux are then evaluated from Eq. (2.4), with which the Grad's 13 distribution function gives the approximated non-equilibrium state. In the meantime, the coefficients in Eqs. (4.6a)-(4.6c) can also be calculated, based on which the new distribution function would be obtained. Comparisons of these results are shown in Fig. 1. It turns out that the new distribution function is more accurate than the Grad's 13 distribution function.

Now we level up the problem to a more practical two-dimensional condition. More expansion terms, including $a_{010}C_2$, $a_{110}C_1C_2$, $a_{030}C_2^3$, $a_{210}C_2C_1^2$, $a_{012}C_2C_3^2$, emerge. The compatibility conditions and moment relationships are still used to determine the co-

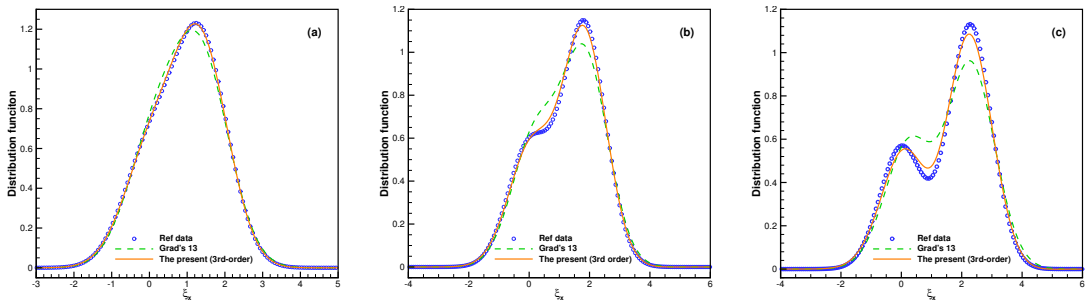

Figure 1: The comparison of the curve shape of distribution functions.

efficients. Their expressions are listed as

$$a_{010}=-\frac{\langle C_2C^2f\rangle}{2\rho(RT)^2},\quad a_{110}=\frac{\langle C_1C_2f\rangle}{\rho(RT)^2}, \tag{4.9a}$$

$$a_{030}=\frac{\langle C_2^3f\rangle}{6\rho(RT)^3},\quad a_{210}=\frac{\langle C_1^2C_2f\rangle}{2\rho(RT)^3},\quad a_{012}=\frac{\langle C_2C_3^2f\rangle}{2\rho(RT)^3}. \tag{4.9b}$$

Numerical tests have been carried out on a recently developed platform called "novel solver" [21–23]. The key issue for this platform is how to accurately construct distribution function at the cell interface. In the conventional "novel solver", the distribution function is obtained by a combination of Grad's 13 distribution function and equilibrium distribution with a weight factor. Thus, on this platform, one just needs to replace the Gard's 13 distribution function with the newly derived distribution function to retrieve the results and make comparisons. The problem configuration here is the flow arising from bottom heated transfer [24] at Knudsen number Kn=0.05, 0.13 and 0.3. This Kn is equivalent to a typical non-equilibrium condition for vehicles (with the characteristic length equal to 1m) at the altitude of 94.2km, 99.5km and 104.5km. The reference viscosity μ_∞ is calculated by $\mathrm{Kn}\cdot L\cdot\rho_\infty\sqrt{RT_\infty}$, where L is the characteristic length, ρ_∞ is the reference density and T_∞ is the reference temperature. In the simulation progress, the Gauss–Hermite quadrature with 28×28 mesh points is utilized for the approximation of numerical integration. As illustrated in Fig. 2, the streamlines predicted by the new distribution function match better with those of discrete velocity method (DVM) [25] than the Grad's 13 [21] distribution function for Kn=0.05. The quantitative comparison of temperature profiles along the central line is plotted in Fig. 3. The results obtained by the new distribution function are also in better agreement with the reference data than those obtained by the Grad's 13 distribution function. A validation of the grid independence for the present solver is conducted by using four sets of mesh scale, including 20×20, 40×40, 60×60 and 80×80. As illustrated in Fig. 4, the results obtained by the mesh scale of 60×60 could converge to the results by 80×80. Thus, 60×60 is fine enough to ensure the simulation accuracy. Fig. 5

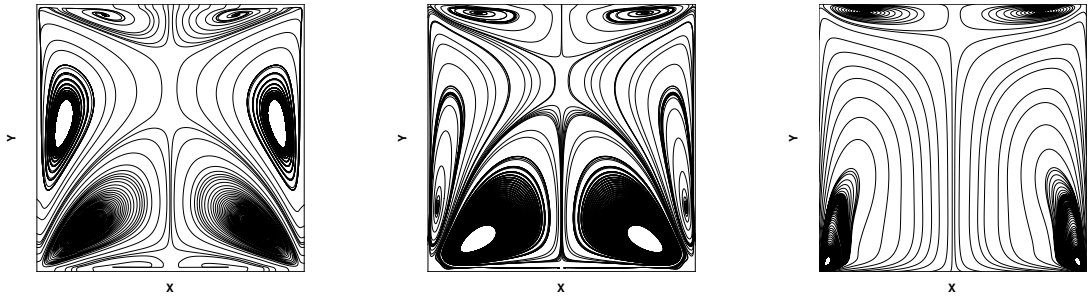

(a) By DVM (b) By 3rd-order (c) By Grad-13

Figure 2: The comparison of streamlines for Kn$=0.05$.

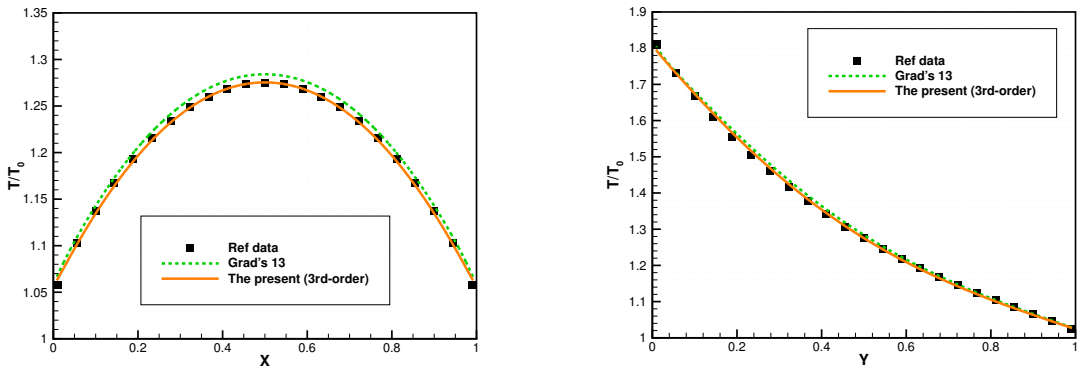

(a) (b)

Figure 3: The comparison of temperature profiles along horizontal central line (a) and vertical central line (b) for Kn$=0.05$.

shows the comparison of streamline for Kn$=0.13$. Reasonable agreements have been obtained between DVM and the present solver. The temperature profiles along horizontal central line and vertical central line are shown in Fig. 6. It can be seen that the results of the present solver match well with those of DVM, but the results based on the Grad's 13 distribution function over-predict the temperature. As displayed in Fig. 7, the flow pattern given by new distribution function is still in better agreement with DVM than the Grad's 13 distribution function. Fig. 8 shows that temperature profiles obtained by the present distribution function are also closer to those given by DVM than the Grad's 13 distribution function.

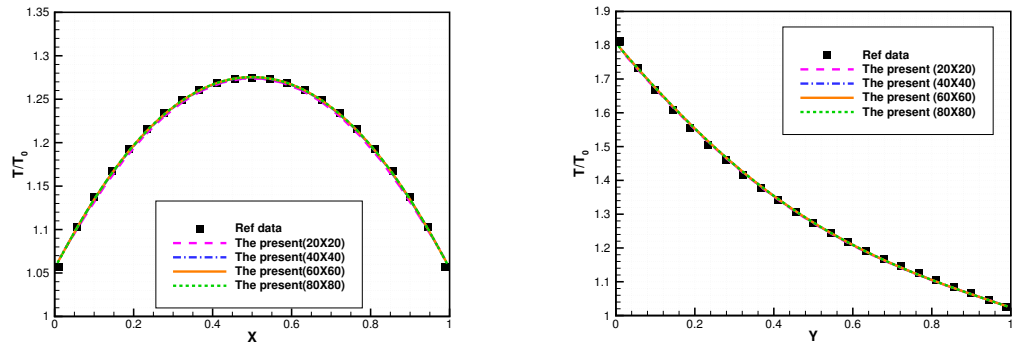

(a) (b)

Figure 4: The comparison of temperature profiles along horizontal central line (a) and vertical central line (b) with different mesh scales.

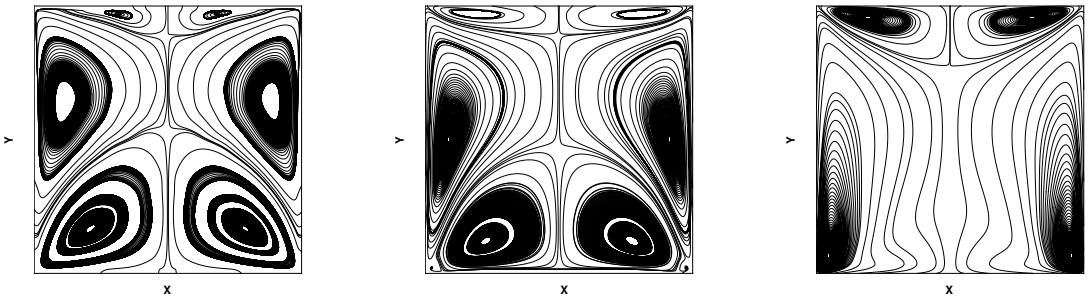

(a) By DVM (b) By 3rd-order (c) By Grad-13

Figure 5: The comparison of streamlines for Kn$=0.13$.

5 Distribution function derived from the fourth-order truncation

In this section, the expanded distribution function will be truncated at the fourth-order to strengthen its capability of simulating non-equilibrium flows. Compared with the derivations in the previous section, more terms that satisfy the condition of $m+n+l=4$ should be considered, which gives the following non-equilibrium term ϕ^{4th}

$$\phi^{4th}=\phi^{3rd}+\sum_{m+n+l=4} a_{mnl}C_1^m C_2^n C_3^l. \tag{5.1}$$

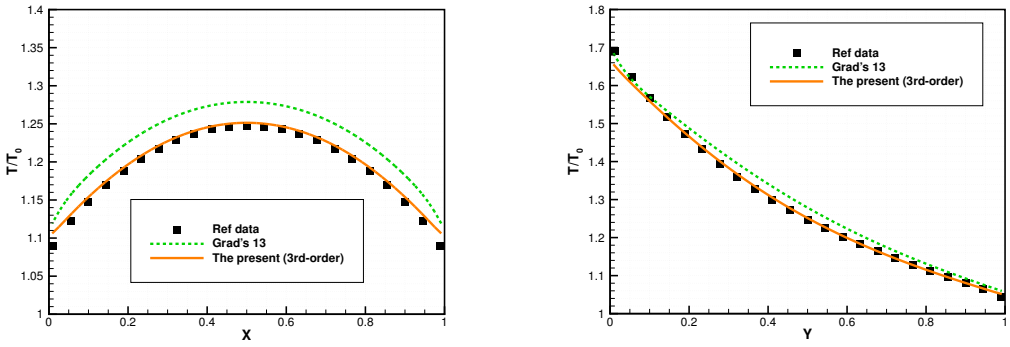

(a) (b)

Figure 6: The comparison of temperature profiles along horizontal central line (a) and vertical central line (b) for Kn=0.13.

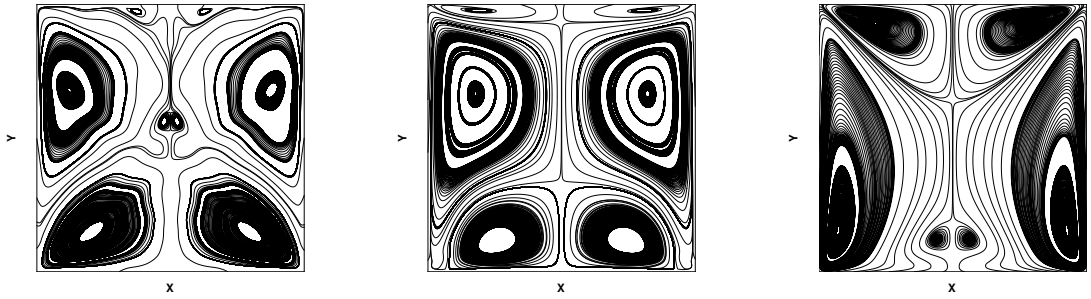

(a) By DVM (b) By 3rd-order (c) By Grad-13

Figure 7: The comparison of streamlines for Kn=0.3.

For simplicity, this process is implemented on the one-dimensional case first, and the term

$$\sum_{m+n+l=4} a_{mnl} C_1^m C_2^n C_3^l$$

can be explicitly written as

$$\sum_{m+n+l=4} a_{mnl} C_1^m C_2^n C_3^l = a_{400} C_1^4 + a_{040} C_2^4 + a_{004} C_3^4 + a_{220} C_1^2 C_2^2 + a_{202} C_1^2 C_3^2 + a_{022} C_2^2 C_3^2. \quad (5.2)$$

Based on the compatibility conditions in Eq. (3.4) and the moment relationships in Eq. (3.5), the coefficients involved in ϕ^{4th} can be derived. It should be noted that some coefficients, including a_{100}, a_{300}, a_{111}, a_{120}, a_{102}, share the same expressions as shown in

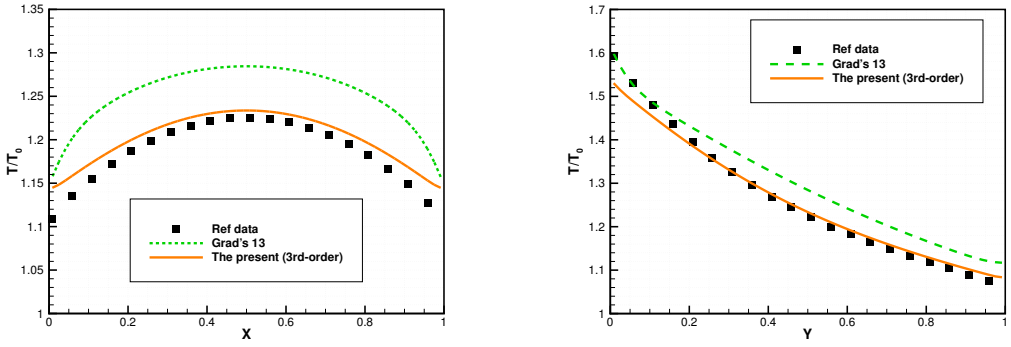

(a) (b)

Figure 8: The comparison of temperature profiles along horizontal central line (a) and vertical central line (b) for Kn=0.3.

Eqs. (4.6a)-(4.6c). Other coefficients are derived as

$$a_{000}=1+\Delta_{000}, \tag{5.3a}$$

$$a_{200}=\frac{\langle C_1C_1f\rangle}{2\rho(RT)^2}-\frac{1}{2RT}-\Delta_{200},\quad a_{020}=\frac{\langle C_2C_2f\rangle}{2\rho(RT)^2}-\frac{1}{2RT}-\Delta_{020},$$

$$a_{002}=\frac{\langle C_3C_3f\rangle}{2\rho(RT)^2}-\frac{1}{2RT}-\Delta_{002}, \tag{5.3b}$$

where

$$\Delta_{000}=(3(a_{400}+a_{040}+a_{004})+(a_{220}+a_{202}+a_{022}))(RT)^2, \tag{5.4a}$$

$$\Delta_{200}=(6a_{400}+a_{220}+a_{202})RT,\quad \Delta_{020}=(6a_{040}+a_{220}+a_{022})RT,$$

$$\Delta_{002}=(6a_{004}+a_{202}+a_{022})RT, \tag{5.4b}$$

$$a_{400}=\frac{\langle fC_1^4\rangle-6(RT)\langle C_1^2f\rangle}{24\rho(RT)^4}+\frac{1}{8(RT)^2}, \tag{5.4c}$$

$$a_{040}=\frac{\langle fC_2^4\rangle-6(RT)\langle C_2^2f\rangle}{24\rho(RT)^4}+\frac{1}{8(RT)^2}, \tag{5.4d}$$

$$a_{004}=\frac{\langle fC_3^4\rangle-6(RT)\langle C_3^2f\rangle}{24\rho(RT)^4}+\frac{1}{8(RT)^2}, \tag{5.4e}$$

$$a_{220}=\frac{\langle C_1^2C_2^2f\rangle-(RT)\langle C_1^2f\rangle-(RT)\langle C_2^2f\rangle}{4\rho(RT)^4}+\frac{1}{4(RT)^2}, \tag{5.4f}$$

$$a_{202}=\frac{\left\langle C_1^2C_3^2f\right\rangle-(RT)\left\langle C_1^2f\right\rangle-(RT)\left\langle C_3^2f\right\rangle}{4\rho(RT)^4}+\frac{1}{4(RT)^2}, \tag{5.4g}$$

$$a_{022}=\frac{\left\langle C_2^2C_3^2f\right\rangle-(RT)\left\langle C_2^2f\right\rangle-(RT)\left\langle C_3^2f\right\rangle}{4\rho(RT)^4}+\frac{1}{4(RT)^2}. \tag{5.4h}$$

To validate the accuracy of the fourth-order truncated distribution function, we adopt the distribution functions shown in Eq. (4.7) again and construct three non-equilibrium distribution functions with the settings of $\hat{\rho}_1=1$, $Ma_1=0$, $\hat{T}_1=1$ and (a) $\hat{\rho}_2=1$, $Ma_2=1.5$, $\hat{T}_2=1$, (b) $\hat{\rho}_2=1$, $Ma_2=2$, $\hat{T}_2=1$, (c) $\hat{\rho}_2=1$, $Ma_2=2.5$, $\hat{T}_2=1$. The implementation is the same as the validation case in Section 4. Comparisons of the recovered distribution functions are shown in Fig. 9. The simulated cases possess quite strong non-equilibrium effects, due to which the results obtained by the third-order truncated distribution function are not satisfactory: in Fig. 9(a), it overestimates the peak value; in Fig. 9(b), it fails to predict the Bimodal effect; in Fig. 9(c), it underestimates the peak values. In comparison, given its enhanced capability of describing non-equilibrium effect, the fourth-order truncated distribution function agrees well with the reference data. Considering that the Grad's 26 distribution function is also truncated at the fourth-order (of Hermite polynomial), its results are also presented in the plots for comparison. In all cases, the results of the Grad's 26 distribution function are less accurate than the present fourth order truncated distribution function, which demonstrates the superiority of the proposed method in constructing distribution functions that can better cope with the non-equilibrium effects.

Now we generalize the fourth-order truncated distribution function to the two-dimensional case by considering more expansion terms, including $a_{130}C_1C_2^3$, $a_{310}C_2C_1^3$ and $a_{112}C_1C_2C_3^2$. The coefficients for these terms are still derived from the capability conditions and moment relationships. Their final expressions are given as

$$a_{310}=\frac{\left\langle C_1^3C_2^1f\right\rangle-3(RT)\left\langle C_1C_2f\right\rangle}{6\rho(RT)^4}, \tag{5.5a}$$

$$a_{130}=\frac{\left\langle C_1^1C_2^3f\right\rangle-3(RT)\left\langle C_1C_2f\right\rangle}{6\rho(RT)^4}, \tag{5.5b}$$

$$a_{112}=\frac{\left\langle C_1^1C_2^1C_3^2f\right\rangle-(RT)\left\langle C_1C_2f\right\rangle}{2\rho(RT)^4}, \tag{5.5c}$$

For validation, the simulation of continuum flows in a lid-driven cavity flow at Reynolds number of Re$=$100, 400 and 1000 are conducted. The computational domain is divided uniformly into 60$\times$60, 80$\times$80 and 100$\times$100 cells with the increase of Reynolds number. The particle velocity space is discretized by 8$\times$8 quadrature points by Gauss–Hermite rule. As shown in Figs. 10, 11 and 12, the results of the third and fourth order truncated distribution function agree well with those of Ghia et al. [26]. These test cases prove that the present distribution functions can recover solutions of NS equations in the continuum regime and give the same accurate results.

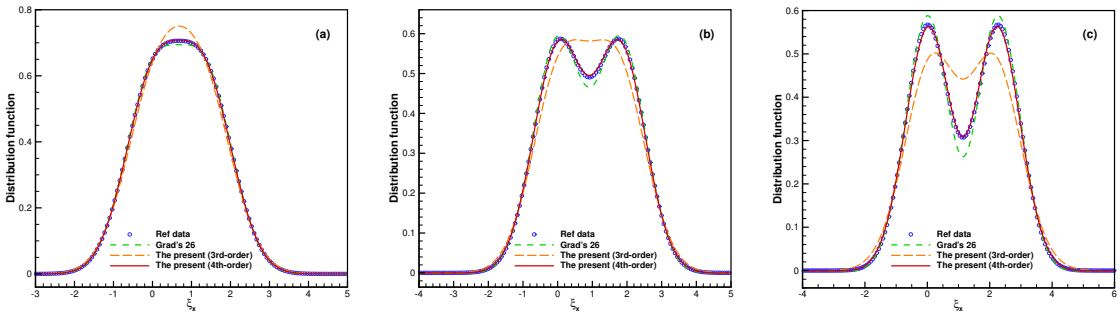

(a) (b) (c)

Figure 9: The comparison of non-equilibrium distribution function profiles.

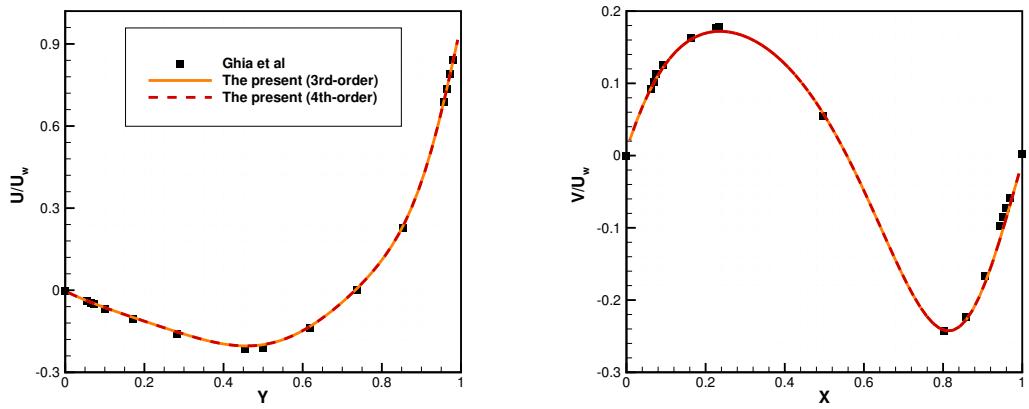

(a) (b)

Figure 10: The comparison of U-velocity (a) and V-velocity (b) profiles along central lines for Re$=$100.

For further validation, we consider a lid-driven cavity flow at Kn$=$ 0.1, which represents a typical non-equilibrium condition for vehicles (with the characteristic length equal to 1m) at the altitude of 98km. The reference viscosity is obtained in the same way as the case of bottom heated transfer flow. For the numerical integration, Gauss-Hermite quadrature with 8×8 mesh points is utilized again. The simulation results are shown in Fig. 13 and compared with the reference results given by the DVM. All of the gas distribution functions predict the anti-Fourier heat transfer phenomenon. As demonstrated in the left plot of Fig. 14, compared with the reference data calculated by DVM, the fourth-order distribution function exhibits higher accuracy in predicting temperature profiles than the other distribution functions. The right plot of Fig. 14 displays the comparison of convergence history between different distribution functions. It is obvious to find that

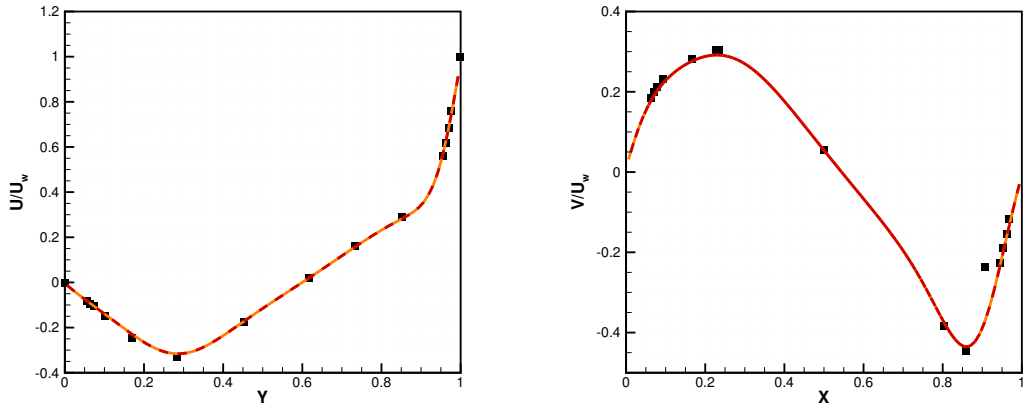

(a) (b)

Figure 11: The comparison of U-velocity (a) and V-velocity (b) profiles along central lines for Re$=$400.

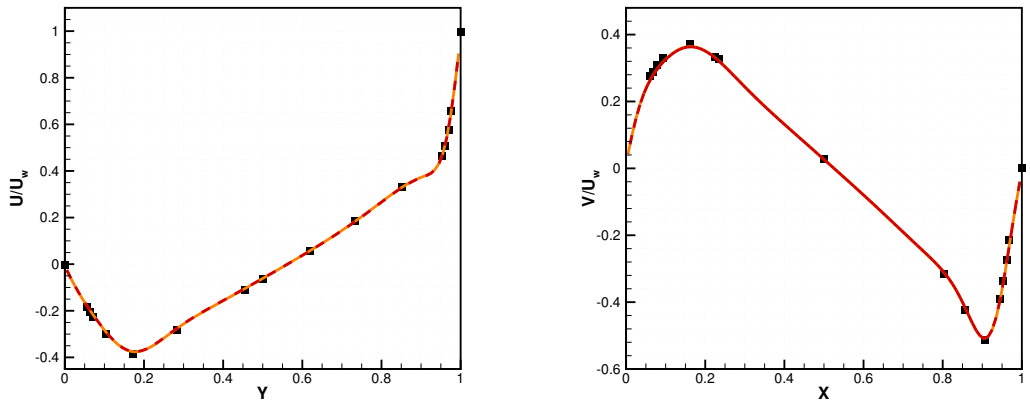

(a) (b)

Figure 12: The comparison of U-velocity (a) and V-velocity (b) profiles along central lines for Re$=$1000.

the convergence rate of present schemes are much faster than that of DVM.

These results validate the capability of the proposed methodology in constructing proper distribution functions for a real non-equilibrium flow problem. Higher order of truncation contributes to the accuracy in predicting stronger non-equilibrium effects, although it is accompanied by more expansion terms. In practice, the truncation order should be determined by the expected non-equilibrium in the investigated problem. For many commonly encountered non-equilibrium flows, the Knudsen number is normally less than 0.1. In such scenario, the present fourth order truncated distribution func-

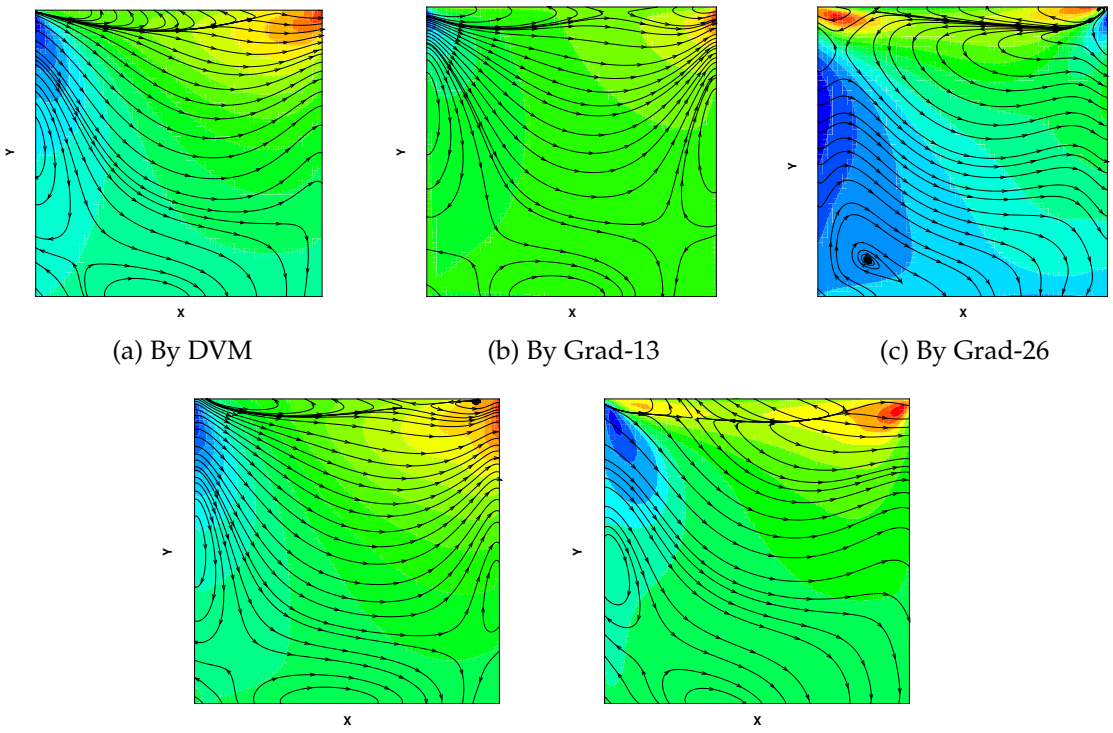

(a) By DVM (b) By Grad-13 (c) By Grad-26

(d) By 3rd-order (e) By 4th-order

Figure 13: The comparison of temperature contours and heat flux lines for Kn$=0.1$.

tion can give satisfactory simulation results and possess better accuracy than the Grad's method truncated at the same order.

6 Conclusions

In this paper, we propose a methodology to construct the non-equilibrium distribution function from a new perspective of polynomial expansion in the peculiar velocity space. The free parameters in the non-equilibrium distribution function can be exactly derived from the compatibility conditions and the moment relationships. The third-order and the fourth-order truncated distribution functions are compared with the Grad's 13 and 26 distribution functions, respectively. The validations of one-dimensional results show that the present method is more accurate than the Grad's method at the same truncation order. Tests of two-dimensional problems are also carried out to forge its prospect in practical applications. Finally, it should be reaffirmed that the proposed methodology can be employed to construct distribution function truncated at higher orders, which would be subject to the strength of non-equilibrium in the investigated problem.

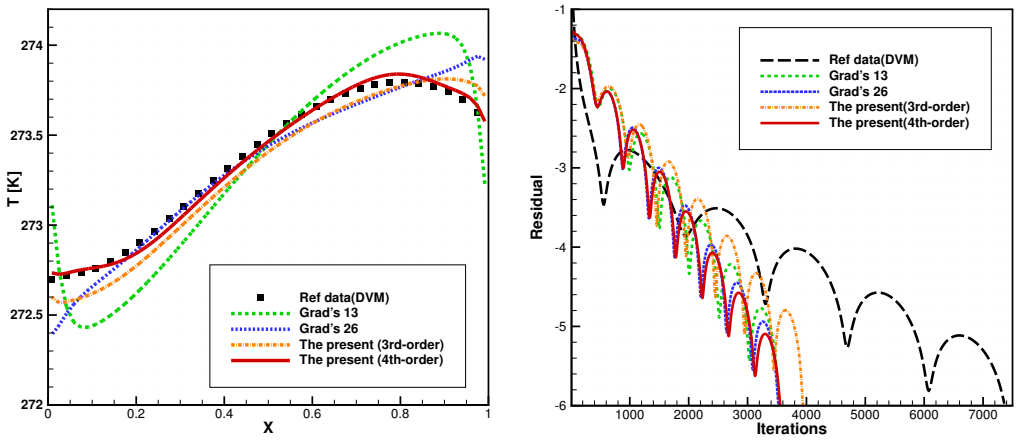

(a) (b)

Figure 14: The comparison of temperature profiles (a) and convergence histories (b) by different distribution functions.

Acknowledgements

The research is partially supported by MOE Tier 1 project at National University of Singapore (No. A-0005235-01-00).

References

[1] J. C. MAXWELL, The Scientific Papers of James Clerk Maxwell, University Press, 1890.
[2] B. GYENIS, *Maxwell and the normal distribution: A colored story of probability, independence, and tendency toward equilibrium,* Studies in History and Philosophy of Science Part B: Studies in History and Philosophy of Modern Physics, 57 (2017), pp. 53–65.
[3] M. AL-GHOUL, AND B. C. EU, *Generalized hydrodynamics and shock waves,* Phys. Rev. E, 56 (1997), p. 2981.
[4] F. URIBE, R. VELASCO, AND L. GARCIA-COLIN, *Burnett description of strong shock waves,* Phys. Rev. Lett., 81 (1998), p. 2044.
[5] M. AL-GHOUL, AND B. C. EU, *Generalized hydrodynamic theory of shock waves in rigid diatomic gases,* Phys. Rev. E, 64 (2001), p. 046303.
[6] S. CHAPMAN, T. G. COWLING, AND D. BURNETT, The Mathematical Theory of Non-Uniform Gases: an Account of the Kinetic Theory of Viscosity, Thermal Conduction and Diffusion in Gases, Cambridge University Press, 1990.
[7] X. SHAN, AND X. HE, *Discretization of the velocity space in the solution of the Boltzmann equation,* Phys. Rev. Lett., 80 (1998), p. 65.
[8] Z. CHEN, C. SHU, Y. WANG, L. YANG, AND D. TAN, *A simplified lattice Boltzmann method without evolution of distribution function,* Adv. Appl. Math. Mech., 9 (2017), pp. 1–22.

[9] Y. LIU, C. SHU, H. ZHANG, AND L. YANG, *A high order least square-based finite difference-finite volume method with lattice Boltzmann flux solver for simulation of incompressible flows on unstructured grids,* J. Comput. Phys., 401 (2020), p. 109019.
[10] H. Z. YUAN, Q. LIU, AND G. ZENG, *An adaptive mesh refinement-multiphase lattice Boltzmann flux solver for three-dimensional simulation of droplet collision,* Int. J. Numer. Meth. Fl., 94 (2022), pp. 443–460.
[11] V. KARA, V. YAKHOT, AND K. L. EKINCI, *Generalized Knudsen number for unsteady fluid flow,* Phys. Rev. Lett., 118 (2017), p. 074505.
[12] H. GRAD, *On the kinetic theory of rarefied gases,* Commun. Pure Appl. Math., 2 (1949), pp. 331–407.
[13] A. RANA, M. TORRILHON, AND H. STRUCHTRUP, *A robust numerical method for the R13 equations of rarefied gas dynamics: Application to lid driven cavity,* J. Comput. Phys., 236 (2013), pp. 169–186.
[14] X. J. GU, AND D. R. EMERSON, *A high-order moment approach for capturing non-equilibrium phenomena in the transition regime,* J. Fluid Mech., 636 (2009), pp. 177–216.
[15] Z. YUAN, L. YANG, C. SHU, Z. LIU, AND W. LIU, *A novel gas kinetic flux solver for simulation of continuum and slip flows,* Int. J. Numer. Meth. Fl., 93 (2021), pp. 2863–2888.
[16] G. M. KREMER, An Introduction to the Boltzmann Equation and Transport Processes in Gases, Springer Science & Business Media, 2010.
[17] L. ZHANG, Z. CHEN, L. YANG, AND M. ZHANG, *An improved axisymmetric lattice Boltzmann flux solver for axisymmetric isothermal/ thermal flows,* Int. J. Numer. Meth. Fl., 90 (2019), pp. 632–650.
[18] Z. YUAN, C. SHU, Z. LIU, L. YANG, AND W. LIU, *Variant of gas kinetic flux solver for flows beyond Navier-Stokes level,* Phys. Rev. E, 104 (2021), p. 055305.
[19] Z. YUAN, C. SHU, AND Z. LIU, *Grad's distribution functions-based gas kinetic scheme for simulation of flows beyond Navier–Stokes level,* Phys. Fluids, 33 (2021), p. 122007.
[20] W. LIU, Y. LIU, L. YANG, Z. LIU, Z. YUAN, C. SHU, AND C. TEO, *Coupling improved discrete velocity method and G13-based gas kinetic flux solver: A hybrid method and its application for non-equilibrium flows,* Phys. Fluids, 33 (2021), p. 092007.
[21] Z. LIU, C. SHU, S. CHEN, L. YANG, M. WAN, AND W. LIU, *A novel solver for simulation of flows from continuum regime to rarefied regime at moderate Knudsen number,* J. Comput. Phys., (2020), p. 109548.
[22] Z. LIU, L. YANG, C. SHU, S. CHEN, M. WAN, W. LIU, AND Z. YUAN, *Explicit formulations of G13-based gas kinetic flux solver (G13-GKFS) for simulation of continuum and rarefied flows,* Phys. Fluids, 33 (2021), p. 037133.
[23] Z. J. LIU, C. SHU, S. Y. CHEN, W. LIU, Z. Y. YUAN, AND L. M. YANG, *Development of explicit formulations of G45-based gas kinetic scheme for simulation of continuum and rarefied flows,* Phys. Rev. E, 105 (2022), p. 045302.
[24] A. S. RANA, A. MOHAMMADZADEH, AND H. STRUCHTRUP, *A numerical study of the heat transfer through a rarefied gas confined in a microcavity,* Continuum Mech. Therm., 27 (2015), pp. 433–446.
[25] L. YANG, C. SHU, J. WU, AND Y. WANG, *Numerical simulation of flows from free molecular regime to continuum regime by a DVM with streaming and collision processes,* J. Comput. Phys., 306 (2016), pp. 291–310.
[26] U. GHIA, K. N. GHIA, AND C. SHIN, *High-Re solutions for incompressible flow using the Navier-Stokes equations and a multigrid method,* J. Comput. Phys., 48 (1982), pp. 387–411.